

RECORDS ADMINISTRATION
R0060858

DP-MS-68-2

671525

NEUTRON RADIOGRAPHY IN BIOLOGICAL MEDIA
TECHNIQUES, OBSERVATIONS, AND IMPLICATIONS

by

Mark Brown
Medical College of Georgia
Augusta, Georgia 30902

and

Paul B. Parke
Savannah River Laboratory
E. I. du Pont de Nemours and Co.
Aiken, South Carolina 29801

SRL
RECORD COPY

Proposed for publication in the
American Journal of Roentgenology

5/23/68

This document was prepared in conjunction with work accomplished under Contract No. AT(07-2)-1 with the U.S. Department of Energy.

DISCLAIMER

This report was prepared as an account of work sponsored by an agency of the United States Government. Neither the United States Government nor any agency thereof, nor any of their employees, makes any warranty, express or implied, or assumes any legal liability or responsibility for the accuracy, completeness, or usefulness of any information, apparatus, product or process disclosed, or represents that its use would not infringe privately owned rights. Reference herein to any specific commercial product, process or service by trade name, trademark, manufacturer, or otherwise does not necessarily constitute or imply its endorsement, recommendation, or favoring by the United States Government or any agency thereof. The views and opinions of authors expressed herein do not necessarily state or reflect those of the United States Government or any agency thereof.

This report has been reproduced directly from the best available copy.

Available for sale to the public, in paper, from: U.S. Department of Commerce, National Technical Information Service, 5285 Port Royal Road, Springfield, VA 22161
phone: (800) 553-6847
fax: (703) 605-6900
email: orders@ntis.fedworld.gov
online ordering: <http://www.ntis.gov/help/index.asp>

Available electronically at <http://www.osti.gov/bridge>

Available for a processing fee to U.S. Department of Energy and its contractors, in paper, from: U.S. Department of Energy, Office of Scientific and Technical Information, P.O. Box 62, Oak Ridge, TN 37831-0062
phone: (865)576-8401
fax: (865)576-5728
email: reports@adonis.osti.gov

NEUTRON RADIOGRAPHY IN BIOLOGICAL MEDIA
TECHNIQUES, OBSERVATIONS, AND IMPLICATIONS

by

Mark Brown
Medical College of Georgia
Augusta, Georgia 30902

and

Paul B. Parks
Savannah River Laboratory
E. I. du Pont de Nemours and Co.
Aiken, South Carolina 29801

INTRODUCTION

Neutron radiography has been used in industrial nondestructive testing for several years¹, though few investigators²⁻⁵ have studied its potential for biological applications. The contrasts in neutron radiographs of biological specimens, however, are sufficiently different from those in roentgenographs so that supplementary information can be obtained.

Neutron radiography, at present, can most easily be performed in the low energy region where both a sufficiently intense neutron source and an efficient neutron visualization system are available. The discussion that follows will center about the special problems of low energy neutron radiography in tissue and review the physical principles involved. The specimens that have been radiographed and displayed have been chosen to illustrate the general properties of neutron images in tissue. The problems of high energy neutron radiography will be discussed in anticipation of the development of an efficient visualization system.

PHYSICS OF LOW ENERGY NEUTRON RADIOGRAPHY IN TISSUE

Penetration. Both photon and neutron radiographic images are the result of local variations in the attenuation of the impinging particle intensity within the media. These variations are governed solely by the linear attenuation coefficients of the materials within the media and by the thickness of the contrasted media.

The average attenuation in tissue of photons is compared to that of neutrons as a function of particle energy in Figure 1. The components of the "standard man"⁶ have been homogenized and normalized with a whole body density of 1.0 gram/cm³ to calculate the linear attenuation coefficients, μ_x and μ_n . Below 10 eV, Barton's³ "bound atom" calculated values are used to normalize the neutron variation. These data show that low energy neutron radiography will probably be restricted to thin tissues (<2.5 cm). Radiography of much greater tissue thicknesses will almost certainly require the greater penetration that can be obtained in the fast neutron region.

Contrast. Low energy neutron radiographs of biological tissue have contrast principally because the density of hydrogen differs in various parts of the sample. The interaction probability of a neutron with a hydrogen nucleus is much larger than with other nuclei, and, furthermore, the hydrogen density is large. On the other hand, in roentgenography the heavier elements attenuate the photons much more than does hydrogen.

Figure 2 compares the photographic densities of muscle, fat, air, and bone in radiographs of a 1-cm-thick sample of round steak produced with thermal neutrons and 15 KVP X-rays. The hydrogen-rich fat in the sample attenuates the neutron beam the most and the X-rays

the least. On the other hand, bone cortex, which is rich in calcium but low in hydrogen, attenuates neutrons the least but X-rays the most. One immediate conclusion is that soft tissue contrasts in neutron radiographs will be relatively free of the bone interference that is so common to roentgenographs.

To choose agents for use in artificially enhancing contrasts in neutron radiographs, the attenuation coefficients of the various elements should be known. Figure 3 compares the linear attenuation coefficient of "standard man" tissue with those of the elements and light and heavy water^{7,8} at thermal energy, 0.025 eV. Figure 4 gives similar data for the most readily recorded epithermal neutron energy, 1.4 eV (the peak of the largest indium resonance).

For the purposes of this report, the terms linear attenuation coefficient and cross section (in units of cm^{-1}) may be used interchangeably. The term absorption coefficient, as generally defined, excludes beam attenuation due to scattering, but is used commonly.

The cross sections in Figures 3 and 4 are for the natural form of these elements. The data can be used to estimate the contrasts attainable with neutron beams of these energies⁹. In principle, similar calculations could be made for roentgenographs, but uncertainty in the X-ray spectrum makes such a calculation difficult.

To induce maximum negative contrasts artificially, the normal tissue medium must be displaced with a substance of an effectively zero attenuation coefficient. From Figures 3 and 4 it is obvious that any gas can be used to approximate this condition. Another relatively biologically safe contrast agent is D_2O (heavy water), which, like the gases, is effectively transparent to neutrons.

To induce positive contrast artificially, strong neutron absorbers are introduced into the tissue medium. For thermal neutron radiography, boron, cadmium, samarium, europium, and gadolinium are the best substances if maximum contrast is the only criterion (Figure 3). Many individual isotopes of various elements have much higher cross sections, e.g., ^{157}Gd has an absorption cross section of $7,320 \text{ cm}^{-1}$ in the metallic form. An organic substance dilutely tagged with ^{157}Gd might make a relatively nontoxic positive contrast agent. At the 1.4 eV of the indium resonance, indium, not surprisingly, has the highest cross section.

In neutron radiography, good negative contrast is often easier to realize than positive contrast, a condition not generally experienced in roentgenography. Positive contrast agents are usually injected into a sample in a dilute mixture with some liquid carrier. Thus, the resulting contrast agent has a much smaller cross section than that of the pure element. On the other hand, the negative contrast from displacing soft tissue is proportional to the relatively high cross section of the tissue alone. Therefore, for low energy neutron radiography the possible positive contrast [μ (agent) - μ (tissue)] is often less than the possible negative contrast [μ (tissue)], where μ is the symbol for cross sections (cm^{-1}). In roentgenography, this effect is usually reversed because the cross section for conventional X-rays in tissue is much lower.

Scatter. In tissue, approximately 94% of all thermal neutron interactions are elastic scattering from hydrogen. Since the scattered neutrons are randomly oriented, they obscure image detail with a dense background fog. This background fog can be handled

in the same manner in which the effect of scattered X-rays is minimized -- by an antiscatter grid. The grid can be constructed by stacking alternate planes of neutron opaque and neutron translucent material chosen for the particular neutron energy under consideration^{5,9}.

EXPERIMENTAL PROCEDURES

Reactor Neutron Source. The Standard Pile (SP) reactor¹⁰ at the Savannah River Laboratory (SRL) was the neutron source for all the neutron radiographs of this report and is shown schematically in Figure 5. The graphite in the core serves to introduce neutrons into the 3-inch-diameter flight tube in the graphite "thermal column", which defines the beam.

For those not familiar with reactors, a general description of reactor neutron beams is included to facilitate an understanding of the terminology. A typical extracted neutron spectrum may be conveniently divided into three adjoining energy regions, thermal, epithermal, and fast, as is shown in Figure 1. The fast and epithermal regions include the fission born neutrons (approximately 2 MeV) and a broad continuous spectrum of partially moderated neutrons down to about 0.5 eV. Below 0.5 eV, the thermal spectrum is usually strongly peaked and is similar to that of a gas in kinetic equilibrium¹¹. This distribution has a peak at about 0.025 eV for room temperature moderators such as the graphite of the SP.

The relative magnitude of the thermal and the epithermal portions of the neutron spectrum varies between different reactor facilities. The images from the two portions of the beam can be

effectively separated by filtration or by selective imaging techniques (discussed later). In this paper, the term thermal radiography will imply the nearly exclusive detection of the Maxwellian portion of the neutron spectrum (whether due to selective imaging or to a weak epithermal content). The term epithermal radiography will imply the nearly exclusive detection of neutrons of energy greater than 0.5 eV (usually due to filtration).

As part of the dose measurements, the flux from the reactor was measured with standard foil techniques¹². At the sample position, the thermal neutron flux was about 3×10^6 n/(cm²)(sec) when the reactor was operated at its maximum power of 8 kW. The total flux over the entire epithermal spectrum was approximately the same. The flux in the energy band from 0.5 to 2.0 eV was about 4×10^5 n/(cm²)(sec). This band is of particular interest in that within it lies the very large indium resonance which is a principle epithermal neutron detector.

Antiscatter Grids. Also shown in Figure 5 are the positions of the sample and the antiscatter grid. The thermal antiscatter grid was assembled by stacking alternate 6 x 1/8-inch strips of 0.008-inch-thick aluminum and 0.005-inch-thick cadmium. The grid ratio was 16:1 with 77 opaque lines per inch. Aluminum is essentially radiolucent to low energy neutrons (Figures 3 and 4), and thus serves as a window for the primary beam neutrons. An epoxy glue held the laminated sections together.

Double grids at 90° opposition were used initially, but eventually only one grid was used because the slight gain in

scattered neutron removal with double grids was obtained only with a considerable loss of line definition due to an accentuation of the penumbra effect. Penumbra was a serious problem because of the reactor's relatively large effective focal spot (discussed later).

The grid frame was designed to fit into the oscillator assembly shown in Figure 6. Low frequency motors and cammed cams were used to impart $3/8$ inch of linear motion to the grid in a plane normal to the grid planes and to the beam. The grid line pattern was therefore blurred and cannot be seen in most of the thermal neutron radiographs.

The antiscatter grid and drive mechanism that was used for the epithermal neutron radiographs was of an earlier design. The grid was assembled by stacking alternate $6 \times 1/2$ -inch strips of 0.032-inch-thick aluminum and 0.005-inch-thick indium. The grid ratio was again 16:1, but with only 27 opaque lines per inch. Moreover, when these radiographs were taken, offset circular cams were used to impart motion to the grid. The resulting sinusoidal motion allowed grid lines to be faintly discernible in the epithermal radiographs. The cadmium-aluminum thermal grid used for Figure 12 was also of this early design.

Image Visualization. Low energy neutrons are poorly absorbed in normal photographic emulsions; thus, in analogy to roentgenography, neutron imaging utilizes converter screens in conjunction with photographic emulsions¹. However, unlike roentgenography, it is not always necessary to have the X-ray film in contact with the converter screen during the neutron irradiation. All of the

neutron radiographs in this report were made by inducing radioactivity on a thin metallic foil that was placed behind the samples. Those neutrons which were unattenuated in the sample produced a radioactive "image" on the foil that subsequently yielded electrons by β decay and internal conversion. The activated foils were removed from the irradiation site, and the images on them were recorded on film by standard autoradiographic techniques. The transfer technique is widely used since almost all neutron beams are contaminated, to some extent, with γ -rays that can cause interfering images. Berger has listed several of the more common transfer converter screens and their physical properties¹.

The detector foil used in thermal transfers is usually made from an activating material with a high cross section and a short half-life. For example, dysprosium, which was used for the thermal transfers of this report, has an activation cross section of 34.9 cm^{-1} and a half-life of 2.3 hours. The detector foil materials for epithermal transfers usually have high activation resonance peaks in the epithermal cross section. Indium, which was used for the reported epithermal transfers, has a very large resonance peak at about 1.4 eV, and, moreover, the activated nuclei have a conveniently short half-life of about 54 minutes. A sheet of 0.032-inch-thick cadmium foil was placed in front of the indium foil to prevent thermal neutrons from activating the indium. The cadmium foil caused no undue loss of epithermal activations because of its low cross section in the epithermal region.

In the transfer technique, Kodak Non-Screen Medical X-ray (NS54T) film was placed in contact with the activated foil in a light-tight cassette for the estimated required film exposure.

The procedure was repeated with new film for an adjusted period in case the first film was incorrectly exposed.

Specimen Preparation. A line definition test phantom was made from a lucite wedge, 1-7/16 inches in its thickest portion, and was constructed so that two negative contrast agents, air and heavy water, and two positive contrast agents, indium and gadolinium, could be tested. These agents were imbedded in the lucite in parallel strips 1/16 inch high to form line pair phantoms of 32, 16, and 8 line pairs to the inch.

Laboratory white rats weighing between 300 and 400 grams were used for most of the tissue specimens. Arteriography specimens were prepared by injecting the contrast media (gadolinium oxide or indium oxide suspended in oil) directly into the aorta. The injection was through a polyethylene catheter (PE 205) inserted by open laparotomy. The animals were sacrificed immediately after the injection. Air and gadolinium oxide contrast media were also introduced in a ventriculography specimen by oysternal puncture. Direct ventricular and lumbar punctures were unsuccessful.

Neutron radiographs of tumor specimens (liposarcoma, breast adenocarcinoma, and uterine leiomyoma) were taken prior to fixation. Control roentgenographs, made in the same plane as the neutron radiographs, were obtained subsequently. All the tumor specimens were approximately 0.3 x 1.0 x 1.0 cm.

Dosimetry. The surface X-ray dose delivered to the various samples was measured with multiple roentgenographic techniques¹³. Comparable neutron doses were estimated from a single foil activation measurement¹² that was made by placing foils on the beam

side of the lucite wedge. The thermal neutron surface dose was about 14 millirads per kilowatt-minute of SP reactor power. The epithermal surface dose in the vicinity of the indium resonance (0.5 - 2.0 eV) was about 2 millirads per kilowatt-minute of SP reactor power; however, this does not include the much larger surface dose from the epithermal neutron spectrum above 2 eV. To minimize the undetected dose from these higher energy neutrons, energy filtration such as can be obtained with crystal spectrometers¹⁴ will be necessary. The gamma surface dose was found to be rather high in our particular reactor, about 71 millirads per kilowatt-minute.

The epithermal and gamma fluxes from the reactor can be greatly diminished, with relatively smaller losses of thermal neutrons, by inserting bismuth and graphite sections into the end of the re-entry tube that is nearest the reactor core. However, since surface dose was not of primary concern during these experiments, the beam from the core was left unaltered. The estimated surface dose of each exposure is listed in Table I.

COMPARISON RADIOGRAPHS

Companion neutron radiographs and roentgenographs are shown for comparison for every specimen. The neutron radiographs were all made in the standard geometry of Figure 5. The radiographic prints in this report have had the very wide range of densities available in the original radiographs compressed by "logetronic"* techniques. This technique was used to preserve as much of the available information on the original films as possible. The

* LogEtronic Incorporated, 7001 Loisdale Rd., Springfield, Va. 22150.

experimental conditions of the radiographs shown in Figures 7-12 are summarized in Table I. Pertinent observations from these figures are detailed in the attached legends. In general, they may be summarized as follows:

1. Positive interference from overlaying bone was minimized in the neutron studies.
2. Negative contrast agents, air and heavy water, produced significantly better contrast with low energy neutrons than with conventional X-ray techniques.
3. Positive contrast agents, gadolinium and indium, were visualized better with conventional X-rays than with low energy neutrons in the tissue studies except where bone interfered.
4. Positive contrast characteristics could be changed markedly with a small change of neutron energy in the low energy region.
5. The soft tissue contrasts seen in the tumor radiographs were greater when studied with neutrons.
6. The maximum tissue penetration from low energy neutrons for effective radiographs was about 2.5 cm.
7. The large dimension of the neutron emitting surface within the reactor introduced a penumbra problem that compromised definition.

DISCUSSION

The elimination of the interfering bone shadows follows simply from the relatively low hydrogen content of osseous structures. The improved visualization of air, however, is fortuitous. The air contrasts with neutron and photon beams which have the same

mean free paths in tissue should be identical. The mean free path of conventional X-rays is, however, considerably longer than that of low energy neutrons. The visualization of heavy water, on the other hand, is a valid observation. Because of the low toxicity of heavy water, this visualization may have important in vivo applications.

The cause for the greater contrast seen in the neutron radiograph of the tumor specimens remains obscure. A possible explanation may be in Frigerio's observation that many tumors have higher hydrogen content than normal tissues¹⁵.

Neutron imaging techniques should at least be capable of definition comparable to that of conventional roentgen techniques using intensifying screens. However, all of the neutron radiographs of this report suffer from the penumbra constraint inherent in using a large source dimension (focal spot). Three common methods of reducing this penumbra are to increase the distance between the source and sample, or to use a diverging collimator with a small source dimension (point source), or to use a series of parallel small diameter collimators. The relatively low source density at the emitting surface within the SF reactor precluded the use of any of these methods because the exposure times became prohibitively long.

FAST NEUTRON RADIOGRAPHY

The data of Figure 1 show that fast neutrons will be necessary to penetrate most parts of the human body. Medical radiography demands both minimal patient exposure to radiation and relatively short exposure times; thus, both efficient image visualization

systems and intense fast neutron sources are necessary. Efforts to develop efficient visualization systems and antiscatter techniques are currently underway. Sufficiently intense sources of fast neutrons are now available. Small accelerators (Neutron Generators) can provide an intensity of 10^{11} n/sec. The same intensity could be obtained with 42 milligrams of ^{252}Cf , and could be concentrated to approximate a point source. Costs are expected to be competitive when this isotope becomes more readily available^{16,17}.

The general character of the image that may be obtained with the spontaneous fission neutrons from a ^{252}Cf source (average neutron energy 2.3 MeV) can be predicted from the data in Figures 1 and 13. Such a radiograph should be similar to a 63 KeV roentgenograph except that bone tissue will be relatively radio-lucent. As with low energy neutron radiography, hydrogen dominates the contrast (88% of the neutron attenuation in "standard man" is due to elastic scattering from hydrogen at 2.3 MeV). To the extent that certain tumors and organs contain more hydrogen than others, it may be anticipated that their contrast as compared to lung tissue in chest radiographs will be enhanced. Figure 13 also shows that gaseous contrast agents will be far more effective than positive contrast agents.

SUMMARY

Neutron radiographic techniques were studied to determine their applicability to the visualization of biological structures. The basic physical principles were reviewed. Roentgenographs and low energy neutron radiographs of various biological specimens

were compared, and a totally different spectrum of shadows was observed. Bone was found to be radiolucent when using neutrons. Fat and muscle could not be differentiated in neutron radiographs but the fat-air contrasts were enhanced. Heavy water and gaseous compounds were found to be most promising among the new group of contrast agents that was appropriate to neutron radiography. Preliminary dosimetry suggests that patient dose will not rank as the principle factor determining applicability.

If fast neutron visualization systems can be perfected and if ^{252}Cf becomes available at a reasonable cost, neutron radiography may have real applicability to medical diagnostics. It will be particularly valuable where air must be visualized in the presence of bone and soft tissue.

ACKNOWLEDGMENTS

The authors wish to express their sincere appreciation to the following individuals for their many contributions to this project. Many helpful discussions have been held with Drs. G. F. O'Neill, N. P. Baumann, and J. L. Crandall of SRL concerning the physical aspects of our studies. H. Berger and Dr. J. P. Barton of ANL greatly assisted the authors by providing a critical review. The assistance of D. E. Hostetler and the operating crew of the SP reactor at SRL is also gratefully acknowledged. The tumor specimens were supplied by Drs. H. J. Peters and J. Challener of the Medical College of Georgia. We also wish to express our thanks to the Savannah River Operations Office of the AEC for use of SRL facilities in this project.

5/23/68

The information contained in this article was developed during the course of work under Contract AT(O7-2)-1 with the U. S. Atomic Energy Commission.

REFERENCES

1. Berger, H. Neutron Radiography, Elsevier Pub. Co., New York, 1965.
2. Berger, H. and McGonnagle, W. J. "Progress Report on Neutron Radiography," USAEC Report ANL-6279, Argonne National Laboratory, 1962.
3. Barton, J. P. Some Possibilities of Neutron Radiography. Physics in Medicine and Biology, 9, 33 (1964).
4. Thewlis, J. Neutron Radiography. Brit. J. Applied Physics, 7, 345 (1956).
5. Atkins, H. L. Biological Application of Neutron Radiography. Materials Evaluation, 23, 453 (1965).
6. Protection Against Neutron Radiation up to 30 Million Electron Volts, Handbook 63, National Bureau of Standards, 8 (1957).
7. Goldberg, M. D., Mughabghab, S. F., Purohit, S. N., Magurno, B. A., and May, V. A. "Neutron Cross Sections," USAEC Report BNL-325, Suppl. No. 2, 2nd Ed. Vol. 2c, 1966.
8. Davis, M. V. and Hauser, D. T. Thermal-Neutron Data for the Elements. Nucleonics, 16, 87 (1958).
9. Barton, J. P. Contrast Sensitivity in Neutron Radiography. Appl. Mater. Res., 4(2), 90 (1965).
10. Axtmann, R. C., Heinrich, L. A., Robinson, R. C., Towler, O. A., and Wade, J. W. "Initial Operation of the Standard File," USAEC Report DP-32, Savannah River Laboratory, 1953.
11. Glasstone, S. and Edlund, M. C. The Elements of Nuclear Reactor Theory, D. Van Nostrand Co., Inc., New York, 1952, p. 36.
12. Courtesy of G. N. Wright and A. Korba, Savannah River Laboratory (1967).
13. Courtesy of C. M. Clay and G. C. Alread, Department of Radiology, Medical College of Georgia (1968).
14. Barton, J. P. Radiography with Resonance Energy Neutrons. Physics in Medicine and Biology, 10, 209 (1965).
15. Barton, J. P. State of the Art-Review, Neutron Radiography - Biological Aspects. Neutron Radiography Newsletter, No. 7, 11 (1967).
16. Stoddard, D. H. "Radiation Properties of Californium-252," USAEC Report DP-986, Savannah River Laboratory, 1965.
17. Reinig, W. C., Savannah River Laboratory, private communication (1967).

18. Report of the International Commission of Radiological Units and Measurements (ICRU), Handbook 62, National Bureau of Standards (1957).
19. Taylor, L. S. The Determination of X-ray Quality by Filter Methods. Radiology, 29, 22 (1957).
20. Glasser, O., Quimby, E. H., Taylor, L. S., Weatherwar, J. L., and Morgan, R. H. Physical Foundations of Radiology, Paul B. Hoeber, Inc., New York, 3rd Ed., 1961, p. 254.

TABLE I
PHYSICAL FACTORS FOR RADIOGRAPHS

Figure	Sample	Detected Energy	Detector	Grid	Neutron Radiography		Fraction of Available Decay Recorded on Film	Adjusted Surface Dose* (rad)	Mean Free Path (mm tissue)
					Neutron Exposure (KV-min)	Detected Thermal or Epithermal Surface Dose (rad)			
2	Round Steak	Thermal	Dy.	1/8" Cd-A1	160	2.2	.25	0.6	3.0
7	Rat Chest	Thermal	Dy.	1/8" Cd-A1	400	5.6	1.0	5.6	3.0
8	Tumor Specimens	Thermal	Dy.	1/8" Cd-A1	120	1.7	.13	0.2	3.0
9	Idne Definition Test Wedge	Thermal	Dy.	1/8" Cd-A1	120	1.7	1.0	1.7	3.0
		Epithermal	In	1/2" In-A1	480	1.0	.75	0.7	6.9
10	Rat Paw and Tail (Gd ₂ O ₃ in Arteries)	Thermal	Dy.	1/8" Cd-A1	400	5.6	.25	1.4	3.0
11	Rat Head (In ₂ O ₃ in Arteries)	Epithermal	In	1/2" In-A1	400	0.8	1.0	0.8	6.9
12	Rat Head (Air and Gd ₂ O ₃ in Ventricles)	Thermal	Dy.	1/2" Cd-A1	400	5.6	1.0	5.6	3.0

* Calculated by multiplying the measured thermal or epithermal entrance dose by the fraction of available decay actually used for the autoradiograph.

TABLE I (Contd)

Roentgenographs

Figure	Sample	Technique	KVP	MA	sec	HVL (mm Al) ¹³ $\frac{HVL_1}{HVL_2}$	Exposure Rate (R/min)	Filter	FSD	Sample Backing	Estimated Entrance Dose (rads) ^{18,*}	Approximate Mean Free Path (mm tissue) ^{19,20}	Equivalent Constant Potential (KV) ^{19,20}
2	Round Steak	0.5 mm Be Window- panatomic X	15	5	1200	0.06	0.06	None	15.5"	None	720	3-5	12
7	Rat Chest	Conventional Mammography	20	300	4	0.34	0.36	None	30"	None	3.0	15	20
8	Tumor Specimens	Conventional Mammography	24	300	4	0.34	0.42	None	30"	None	3.7	20	23
9	Long Defini- tion Test Wedge	Conventional Monoscreen	45	20	5	1.2	1.7	2 mm Al	40"	None	0.2	44	42
10	Rat Paw and Tail (Gd ₂ O ₃ in Arteries)	Conventional Monoscreen	45	20	5	1.2	1.7	2 mm Al	40"	0.031 [*] Al	0.2	44	42
11	Rat Head (InG ₂ O ₃ in Arteries)	Conventional Monoscreen	45	20	5	1.2	1.7	2 mm Al	40"	0.031 [*] Al	0.2	44	42
12	Rat Head (Gd ₂ O ₃ in Ventricles)	Conventional Monoscreen	60	20	0.08	1.4	1.5	2 mm Al	40"	0.031 [*] Al	0.1	50	55

* Assumptions: Water density tissue; ICRU (1956) rads to roentgen conversion factors¹⁹ at KVP meter readings; NO corrections for effective KVP or backscatter were made.

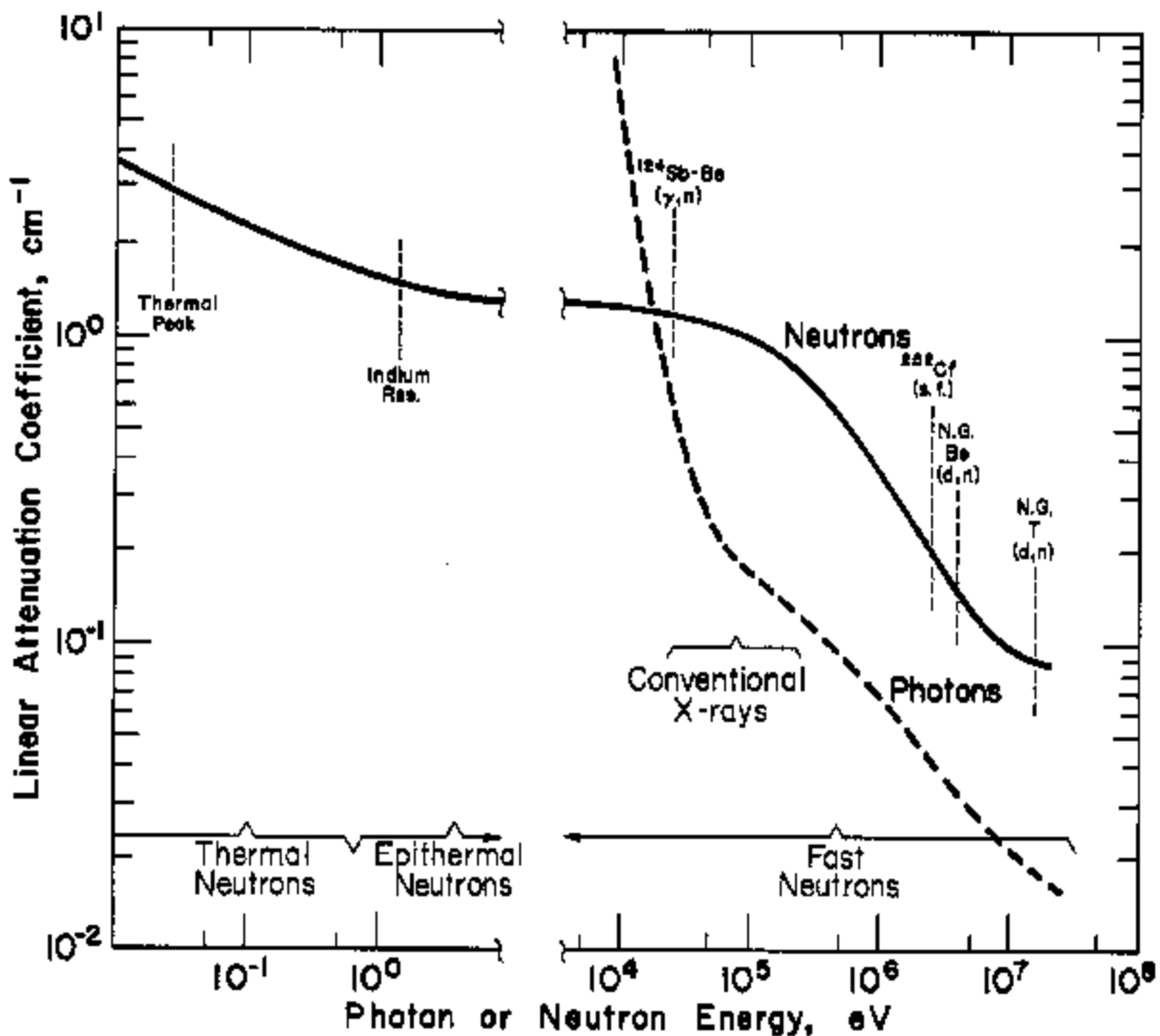


FIG. 1 Linear Attenuation Coefficients of Neutrons and Photons in Standard Man Tissue (Density = 1.0 g/cm³)
 The low energy and fast neutron source ranges and corresponding attenuation coefficients are shown. These are compared to photon attenuation coefficients. Note that the conventional X-ray penetration can be duplicated only with fast neutrons. Low energy neutron radiography must be restricted to thin specimens.

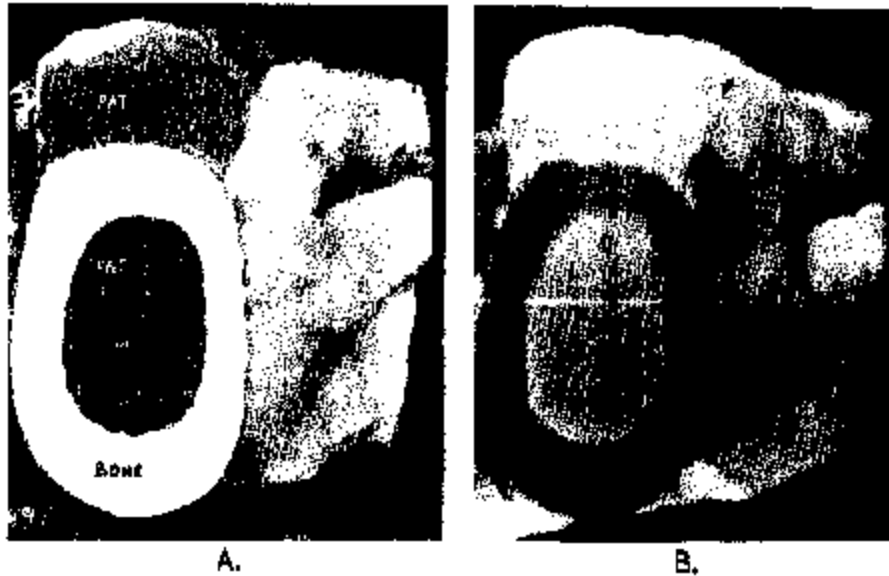


FIG. 2 Comparison of Thermal Neutron Radiograph (right) and 15 KVP Roentgenograph of a Round Steak Specimen (1 cm thick)

The elastic scattering of neutrons from the hydrogen nucleus is primarily responsible for the attenuation of neutrons in tissue, whereas the absorption and scattering of X-rays in heavier elements dominate the photon attenuation. Thus, while hydrogen rich fat yields maximum neutron attenuation, minimum photon attenuation is observed. The reverse occurs in hydrogen deficient bone. The fat-air contrast is superior in the neutron radiograph but the muscle-fat contrast is superior in the roentgenograph.

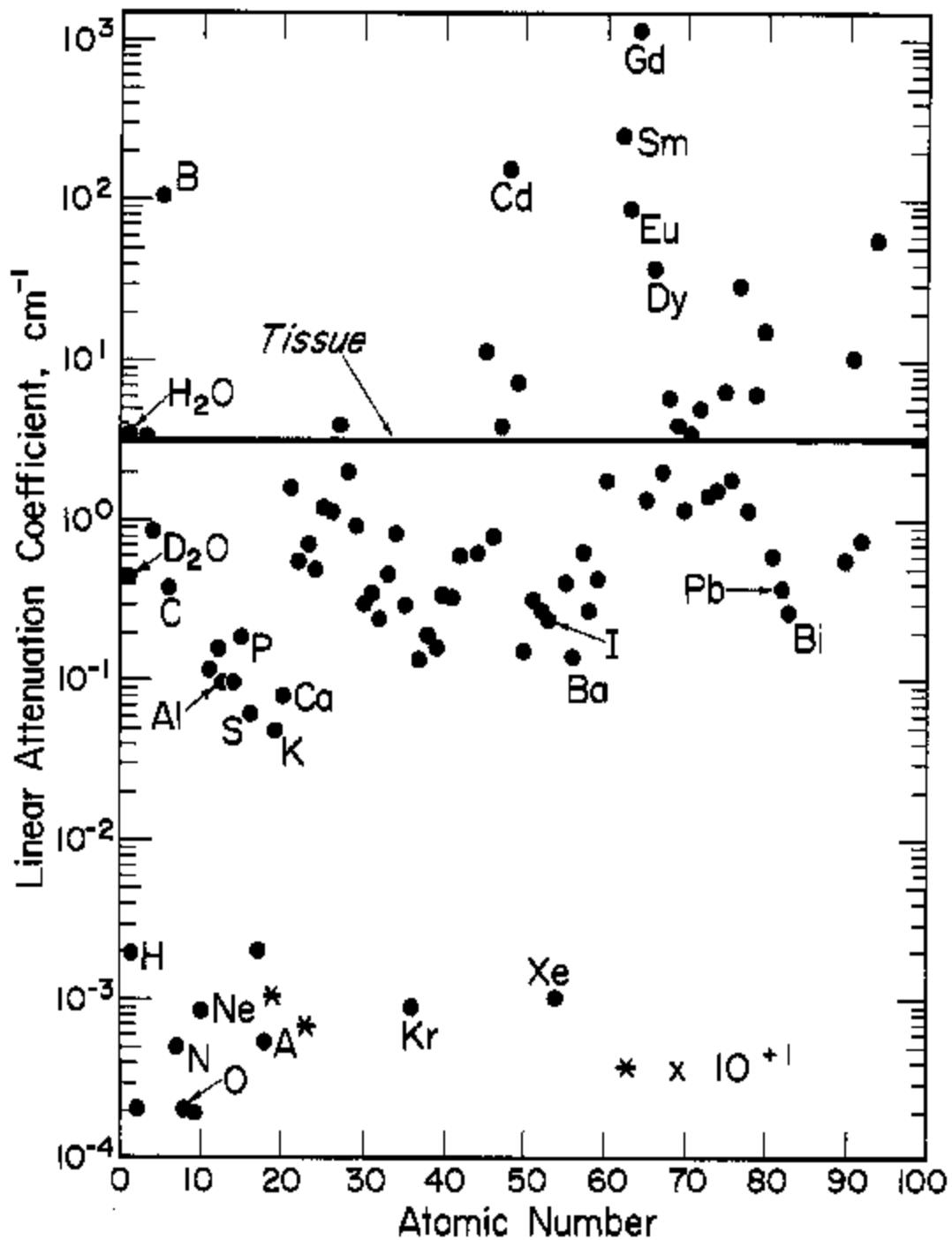


FIG. 3 Thermal Neutron (0.025 eV) Linear Attenuation Coefficients of Natural Elements (and Light and Heavy Water) vs Standard Man Tissue

Prominent positive contrast agents are boron, cadmium, gadolinium, etc.; prominent negative contrast agents are D₂O (heavy water), air, noble gases, calcium, barium, etc.

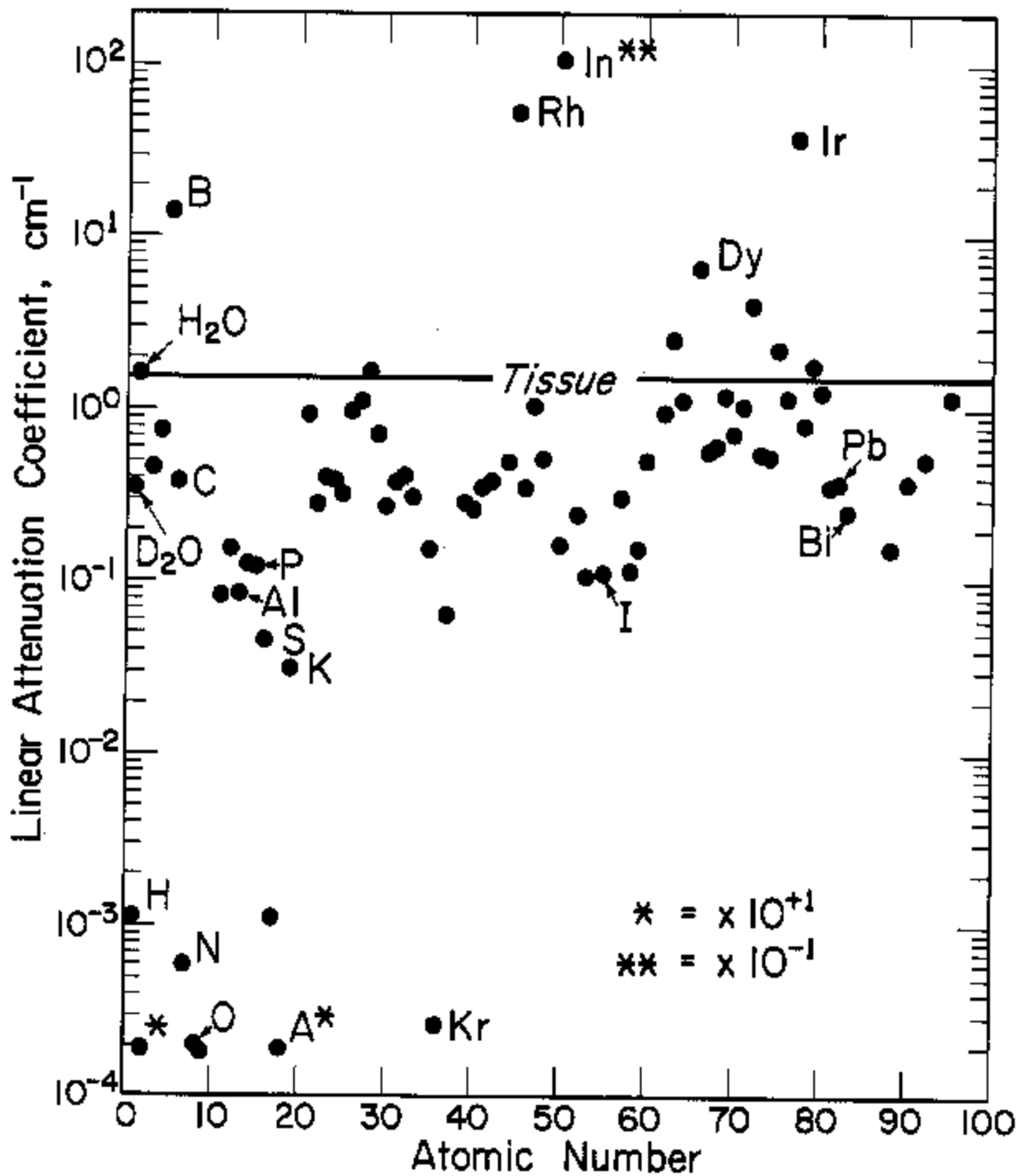


FIG. 4 Indium Resonance (1.45 eV) Linear Attenuation Coefficients of Natural Elements (and Light and Heavy Water) vs Standard Man Tissue
 Prominent positive contrast agents are boron and indium; prominent negative contrast agents are D₂O (heavy water), air, noble gases, etc.

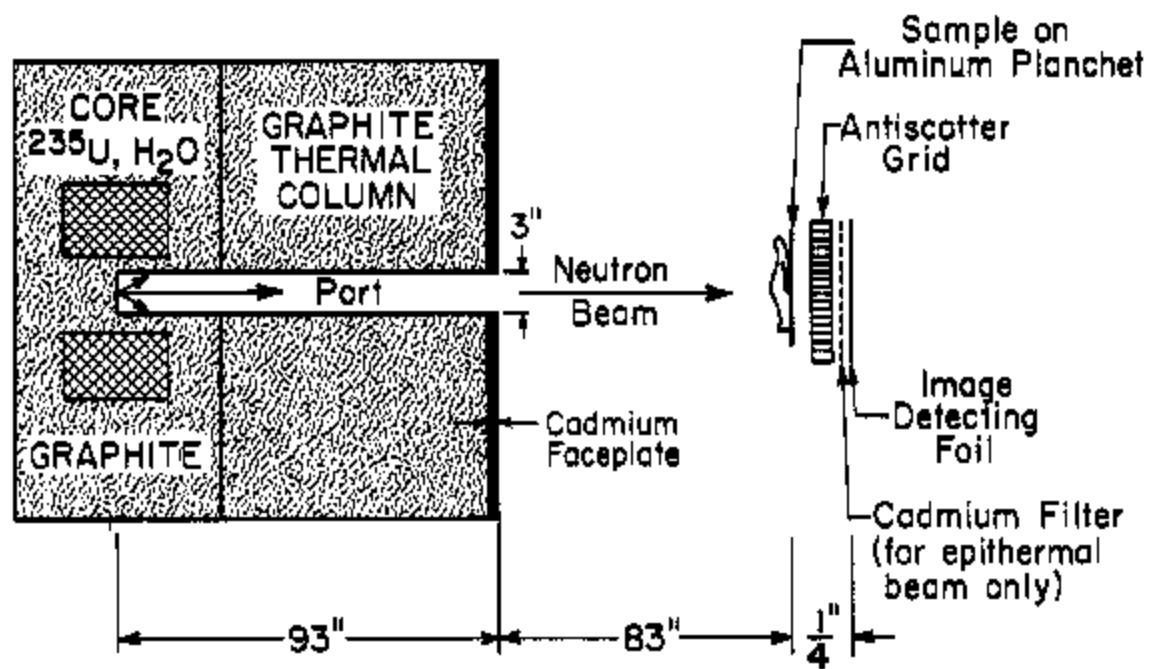


FIG. 5 The Experimental Arrangement for Low Energy Neutron Radiography

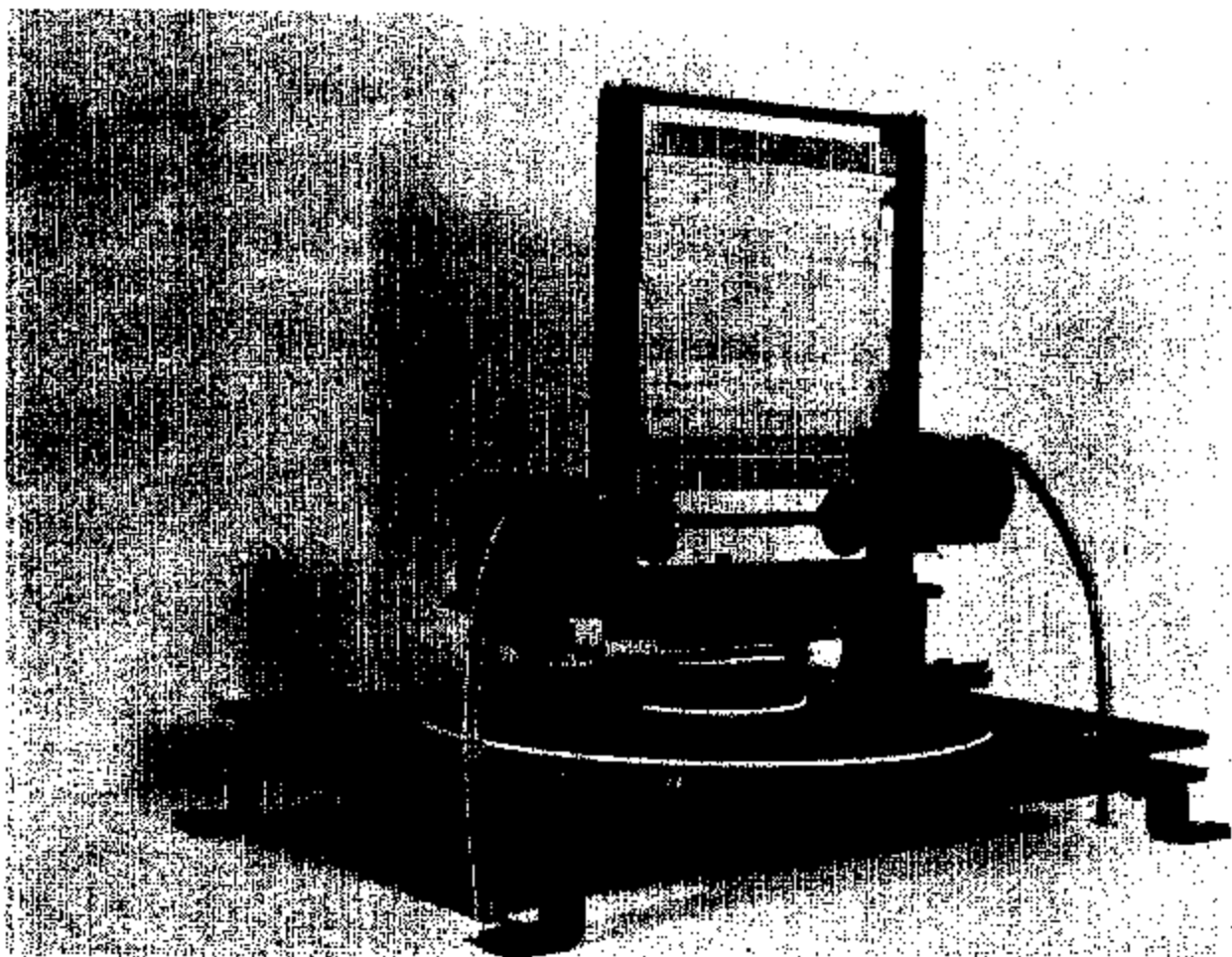
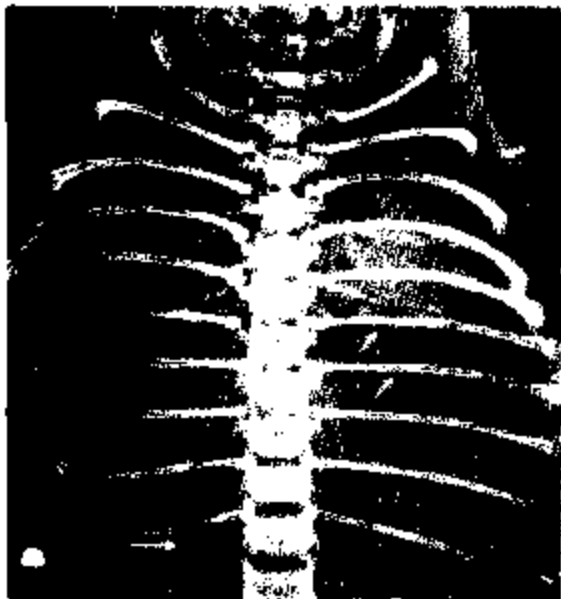


FIG. 6 The Antiscatter Grid and Oscillator



A.



B.

FIG. 7 Comparison Radiographs of the Chest of a Dead Rat

A. High definition, low KV roentgenograph.
B. Neutron radiograph (0.025 eV). The neutron radiograph demonstrates enhancement of the contrast between the air and soft tissues. Note also that the shadows of the overlying bone have disappeared. Air in the pulmonary arteries (↗) as well as within the hepatic vein (↓) and vena cava (→) can be visualized. The relative unsharpness is due to a correctable penumbra problem.

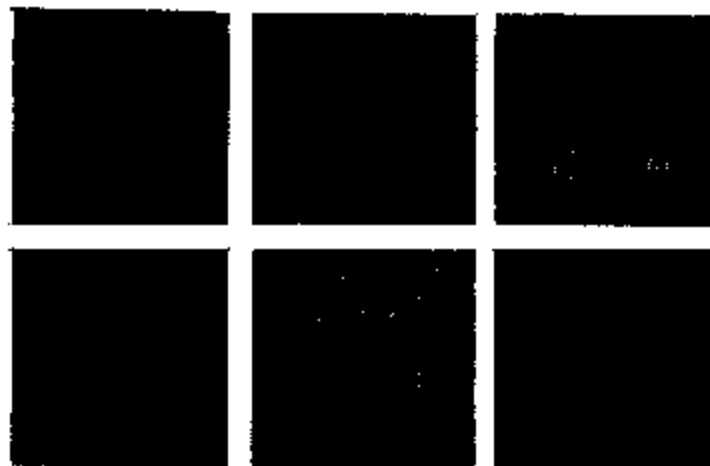


FIG. 8 Tumor Specimen Radiography

Left column, mammary adenocarcinoma. Middle column, liposarcoma. Right column, uterine leiomyoma. The thermal neutron radiographs (top row) are compared to the high definition, low KVP roentgenographs. The patterns depicted by the radiographs are not fully understood.

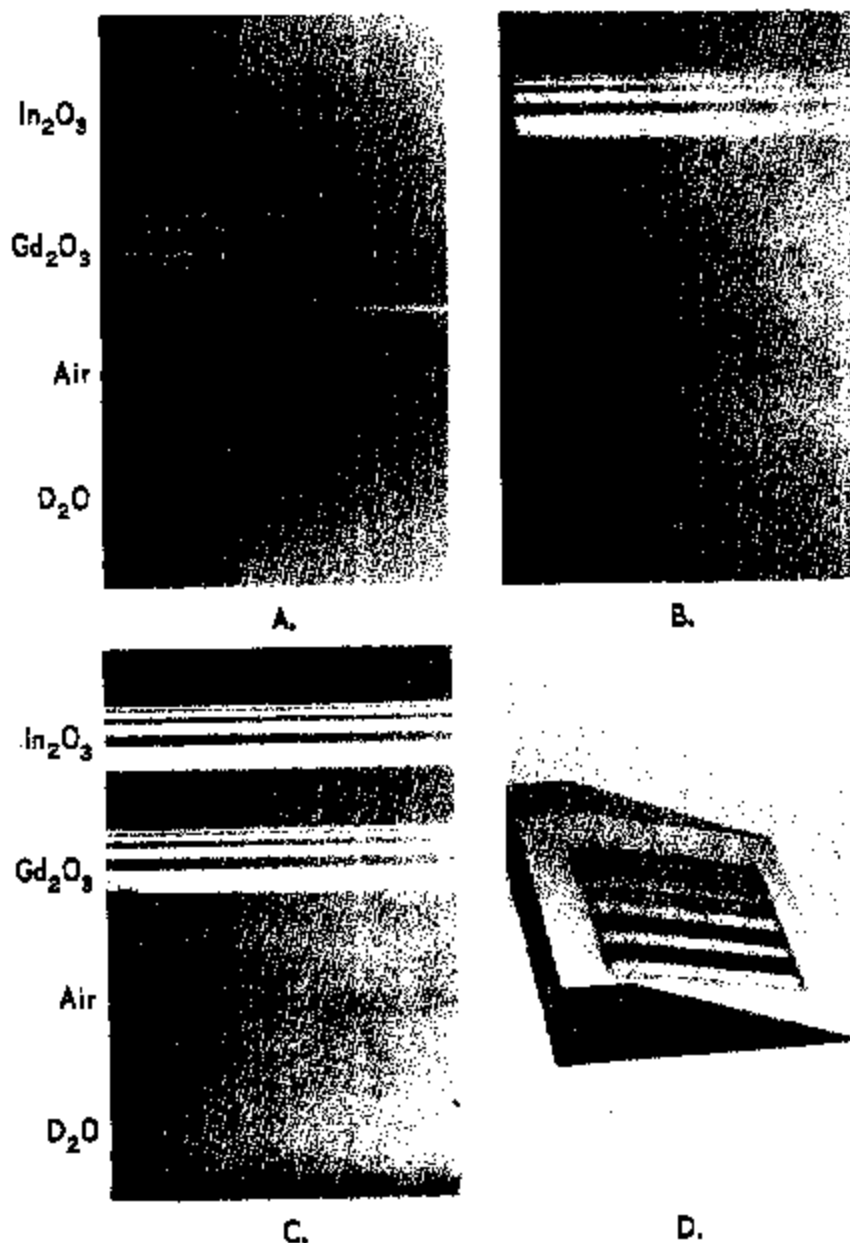


FIG. 9 Tissue Substitute Test Wedge

Two positive contrast agents (Gd_2O_3 and In_2O_3) and two negative contrast agents (air and heavy water) are displayed as 1/16 inch line pair phantoms (B, 16, and 32 L.P./I.) in a lucite test wedge. A. Thermal neutron radiograph (0.025 eV). B. Epithermal neutron radiograph (primarily 1.4 eV). C. Conventional nonscreen roentgenograph. D. Photograph of lucite test wedge. Note the improved contrast of the air shadows and the visualization of heavy water when neutrons are used. Note also the pronounced difference in the contrast offered by gadolinium and indium at the two neutron energies.



A.

B.

FIG 10 Neutron Arteriography

A. Thermal neutron radiograph of a rat paw and tail. B. Conventional nonscreen roentgenograph. Gd_2O_3 in oil was the contrast agent. The superior definition on the roentgenograph is compensated for by the complete absence of any bone shadow interference in the neutron radiograph. Note that several arteries are visualized on the neutron radiograph that are not discernible on the roentgenograph (arrows).

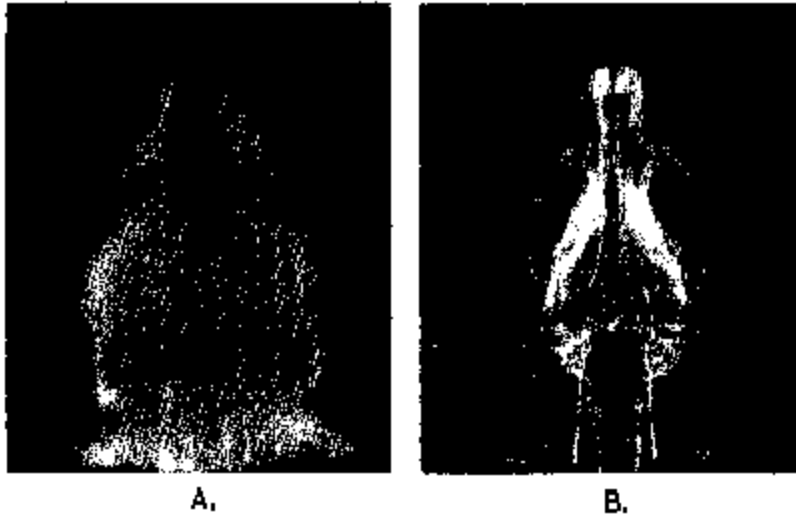
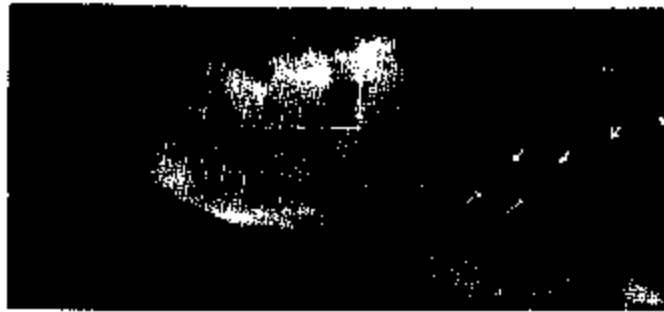


FIG. 11 Cerebral Neutron Arteriography

A. Epithermal neutron radiograph (primarily 1.4 eV). B. Conventional nonscreen roentgenograph. Although the epithermal beam was too weak to demonstrate the In_2O_3 contrast agent intracranially, the negative contrast areas are well seen. The excellent visualization of the nasopharynx with neutrons is due to improved air contrast and the absence of interfering osseous shadows.



A.



B.

FIG. 12 Neutron Ventriculography

A. Thermal neutron radiograph. B. Conventional nonscreen roentgenograph. Both air and Gd_2O_3 were introduced by cisternal puncture. In the neutron radiograph, note the superior visualization of the air in the ventricle (\uparrow), trachea (\nearrow), and spinal canal (\swarrow). The low transmission through the cranial vault (box) is thought to be responsible for the poor contrast offered by the Gd_2O_3 (\downarrow) on the neutron radiograph.

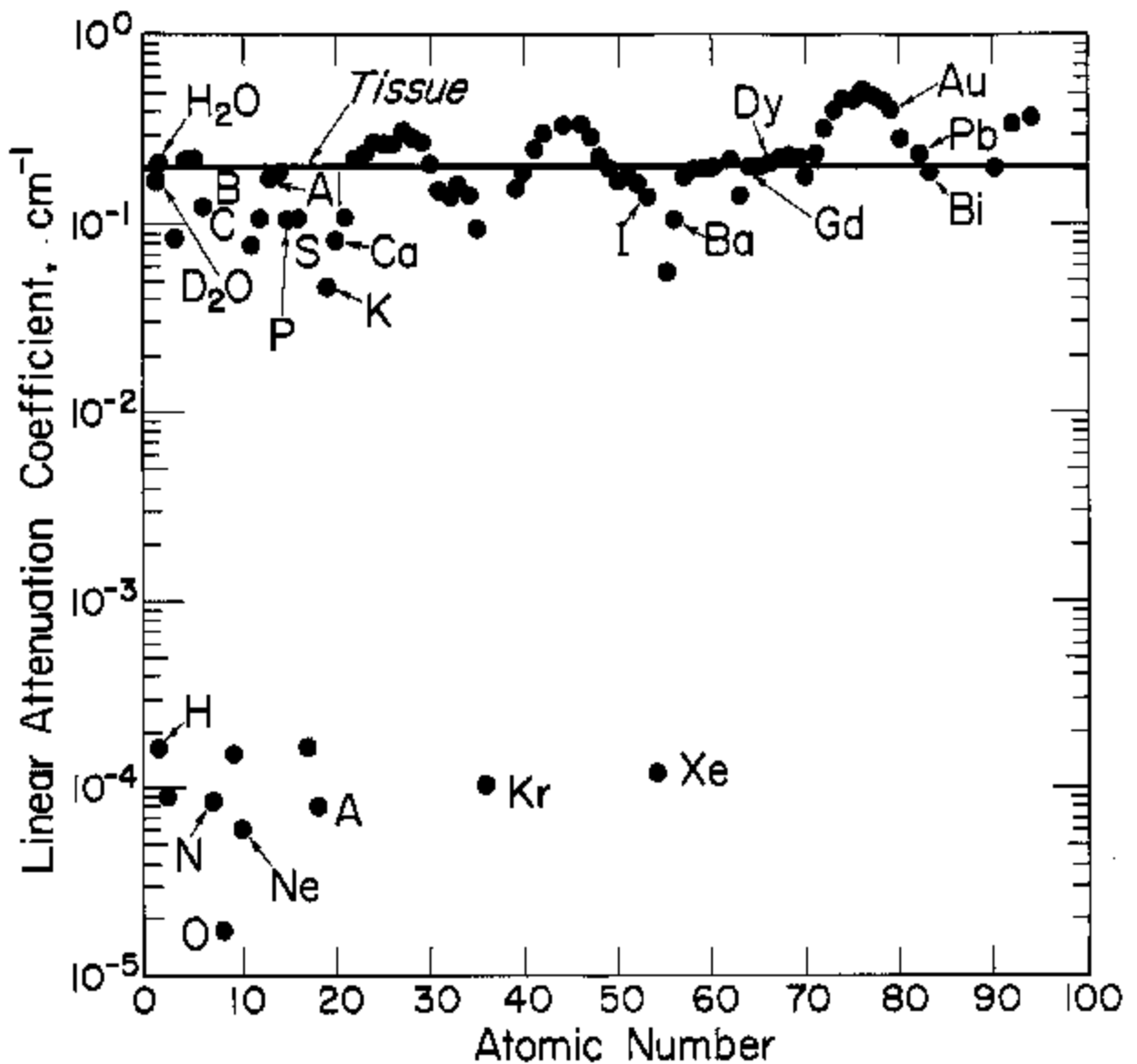


FIG. 13 ²⁵²Cf Source (2.3 MeV Average) Linear Attenuation Coefficients for Natural Elements (and Light and Heavy Water) vs Standard Man Tissue

Note that prominent positive contrast agents do not exist. Negative displacement contrast with gases should approximate the air-tissue contrasts obtained with 63 KV X-rays.